PTEP

Prog. Theor. Exp. Phys. **2019**, 033B04 (14 pages)
DOI: 10.1093/ptep/ptz013

Quark mass function at finite temperature in real-time formalism

Hidekazu Tanaka* and Shuji Sasagawa*

Department of Physics, Rikkyo University, Tokyo 171-8501, Japan
*E-mail: tanakah@rikkyo.ac.jp; dedicatedphys@gmail.com

Received August 9, 2018; Revised January 23, 2019; Accepted February 6, 2019; Published March 30, 2019

We investigate the properties of quark mass functions at finite temperature in quantum chromodynamics calculated by the Schwinger–Dyson equation in the real-time formalism without the instantaneous exchange approximation, in which the loop integration is performed in Minkowski space. In our model, real and imaginary parts of the mass function in the time-like momentum region are directory evaluated. We show that the imaginary part of the mass function has a positive value in some time-like momentum region below the critical temperature for chiral symmetry restoration at finite temperature, which may imply quark confinement.

Subject Index B69

1. Introduction

Chiral phase transition in quantum chromodynamics (QCD) is one of the most interesting phenomena still to be understood. So far, chiral phase transitions have been studied by various methods. One such method is implementation of the Schwinger–Dyson equation (SDE) [1,2], which can evaluate nonperturbative phenomena.

A great deal of work on chiral symmetry breaking has been done with the SDE in the momentum representation, in which a one-loop contribution is integrated over Euclidean space. Some calculations of the mass function for fermions with the SDE have been done in Minkowski space. In Ref. [3], a spectral representation for Green functions is assumed, in which the mass functions are calculated in Lorentz invariant form. In Ref. [4], explicit one-loop contributions of the mass function have been calculated. However, the mass function is evaluated only one iteration from a constant initial mass as an input.

At finite temperature and density for equilibrium systems, the imaginary-time formalism (ITF) is implemented, which continues to Euclidean space at the zero temperature limit. On the other hand, the real-time formalism (RTF) for nonequilibrium systems is formulated in Minkowski space. The SDE in the RTF has been studied with the instantaneous exchange approximation (IEA) [5,6] in which gauge boson energy is neglected. In the IEA, the mass function does not depend on the energy. Furthermore, the critical coupling of chiral symmetry breaking in quantum electrodynamics (QED) is about half that calculated with four-momentum integration in Euclidean space at zero temperature [6–9]. An alternative method was proposed in Ref. [10], in which an energy independence condition for the mass function is required. In evaluation of the mass function, only results for the static limit as momentum $p \to 0$ with zero energy $p_0 = 0$ have been presented [11].

Funded by SCOAP[3]

Analytic continuation from Euclidean space to Minkowski space is valid in perturbative calculations if the pole positions in the complex plane of energy are known. However, it is not trivial in the nonperturbative region, particularly when the mass function depends on the energy. So far, the structure of the quark mass function in the strong coupling region in the entire range of energy and momentum space has not been fully studied in Minkowski space at finite temperature and density. In our previous papers [12,13], we formulated the SDE for QED and QCD, in which the momentum integration is performed in Minkowski space without the IEA.

In Minkowski space, if the imaginary part of the mass function is small, the propagator varies rapidly near resonance peaks, which is one of the difficulties with numerical calculation. In our method, the resonance contributions in momentum integration in Minkowski space are efficiently evaluated. Furthermore, we can directory evaluate real and imaginary parts of the mass function in the time-like momentum region. At zero temperature, we found that the imaginary part of the mass function in some time-like momentum region becomes positive, in which the spectral function has negative value. The positivity violation of the spectral function contradicts the existence of asymptotic fields of the quark [13], which may imply confinement of quarks. Therefore, it is interesting to investigate the imaginary part of the mass function at finite temperature.

In this paper, we extend our previous method to calculate the quark mass functions with the SDE in the RTF at finite temperature without the IEA. In Sect. 2, we formulate the SDE in the RTF. In Sect. 3, some numerical results are shown. Section 4 is devoted to the summary and some comments.

2. SDE for quark mass function

In the RTF, two types of fields specified by 1 and 2 are implemented in the theory, in which the type-1 field is the usual field and the type-2 field corresponds to a ghost field in the heat bath.

We calculate the 1-1 component of a self-energy of quark $\Sigma^{11}(p)$ in QCD, which is given by

$$-i\Sigma^{11}(P) = (ig_{\rm s})^2 C_{\rm F} \int \frac{d^4Q}{(2\pi)^4} \gamma^\mu i S^{11}(Q) \Gamma^\nu i D^{11}_{\mu\nu}(K), \tag{2.1}$$

where S^{11} and $D^{11}_{\mu\nu}$ are the 1-1 components of thermal propagators for a quark with momentum $Q = (q_0, \mathbf{q})$ and a gluon with momentum $K = P - Q = (k_0, \mathbf{k})$, respectively. Here, $P = (p_0, \mathbf{p})$ is an external momentum of the quark. The strong coupling constant and the color factor are denoted by $g_{\rm s}$ and $C_{\rm F} = 4/3$, respectively.

The 1-1 component of the quark propagator in the RTF is given as

$$iS^{11}(Q) = i\left[(S_{\rm F}(Q))_{\rm R} + i(S_{\rm F}(Q))_{\rm I}\epsilon(q_0)\tanh\frac{q_0}{2T}\right] \tag{2.2}$$

with a temperature T, where we define $\epsilon(z) = \theta(z) - \theta(-z)$ with the step function $\theta(z)$. Here, $(S_{\rm F}(Q))_{\rm R}$ and $(S_{\rm F}(Q))_{\rm I}$ are the real and imaginary parts of the quark propagator $S_{\rm F}(Q)$.[1]

[1] The real and imaginary parts of a propagator G are defined by

$$(G)_{\rm R} = \frac{1}{2}(G + G^*)$$

and

$$i(G)_{\rm I} = \frac{1}{2}(G - G^*),$$

respectively.

In this paper, we define the quark propagator as

$$iS_{\rm F}(Q) \equiv i(\not{Q} + M(Q))I_{\rm F}(Q) \tag{2.3}$$

with

$$I_{\rm F}(Q) = \frac{1}{q_0^2 - q^2 - M^2(Q) + i\varepsilon}. \tag{2.4}$$

The 1-1 component of the gluon propagator in the RTF is given as

$$iD_{\mu\nu}^{11}(K) = i\left[(D_{{\rm F}\mu\nu}(K))_{\rm R} + i(D_{{\rm F}\mu\nu}(K))_{\rm I}\epsilon(k_0)\coth\frac{k_0}{2T}\right], \tag{2.5}$$

where

$$iD_{{\rm F}\mu\nu}(K) \equiv P_{\mu\nu}^{\rm L} iD_{\rm L}(K) + P_{\mu\nu}^{\rm T} iD_{\rm T}(K) \tag{2.6}$$

with

$$P_{\mu\nu}^{\rm L} = -g_{\mu\nu} + \frac{K_\mu K_\nu}{K^2} - P_{\mu\nu}^{\rm T} \tag{2.7}$$

and

$$P_{\mu\nu}^{\rm T} = \left(-g_{\mu\nu} + \frac{k_\mu k_\nu}{\mathbf{k}^2}\right)(1-\delta_{0\mu})(1-\delta_{0\nu}), \tag{2.8}$$

where the longitudinal and transverse components of the gluon propagator are given as

$$iD_{\rm L}(K) = \frac{i}{K^2 - m_{\rm L}^2 + i\varepsilon} \tag{2.9}$$

and

$$iD_{\rm T}(K) = \frac{i}{K^2 - m_{\rm T}^2 + i\varepsilon}, \tag{2.10}$$

respectively. Here, $m_{\rm L}$ and $m_{\rm T}$ denote the longitudinal and transverse gluon masses, respectively. The quark–gluon vertex is defined by $\Gamma_\mu = \gamma_\mu$. Our model corresponds to a mass function in the Landau gauge.

Integrating over the azimuthal angle of the momentum $\mathbf{q}$, the trace of the self-energy Σ^{11} is given by

$$M^{11}(P) \equiv \frac{1}{4}Tr[\Sigma^{11}(P)] = -\frac{iC_{\rm F}}{2\pi^2}\int_{-\Lambda_0}^{\Lambda_0} dq_0 \int_\delta^\Lambda dq \frac{q}{p}\alpha_{\rm s}[MI_{11}J_{11}](P,Q) \tag{2.11}$$

with $p = |\mathbf{p}|$, $q = |\mathbf{q}|$, and $\alpha_{\rm s} = g_{\rm s}^2/(4\pi)$, where

$$MI_{11} = (MI_{\rm F})_{\rm R} + i(MI_{\rm F})_{\rm I} N_{\rm F}(T, q_0) \tag{2.12}$$

and

$$J_{11} = (J_{\rm F})_{\rm R} + i(J_{\rm F})_{\rm I} N_{\rm B}(T, k_0) \tag{2.13}$$

with $N_{\rm F}(T,q_0)=\epsilon(q_0)\tanh[q_0/(2T)]$ and $N_{\rm B}(T,k_0)=\epsilon(k_0)\coth[k_0/(2T)]$, and

$$J_{\rm F}=\int_{\eta_-}^{\eta_+}dkk\,[D_{\rm L}(K)+2D_{\rm T}(K)] \tag{2.14}$$

with $\eta_\pm=|p\pm q|$ and $k=|\mathbf{k}|$, respectively.

The real part $M_{\rm R}$ and the imaginary part $M_{\rm I}$ of the mass M are given by

$$M_{\rm R}=(M^{11})_{\rm R} \tag{2.15}$$

and

$$M_{\rm I}=(M^{11})_{\rm I}/N_{\rm F}(T,q_0), \tag{2.16}$$

respectively.

In Minkowski space, if the imaginary part of the mass function $(M^2)_{\rm I}$ is small, the propagator $I_{\rm F}$ in Eq. (2.4) varies rapidly near $Q^2=q_0^2-q^2\simeq(M^2)_{\rm R}$, which is one of the difficulties with numerical calculation in Minkowski space. Therefore, it is necessary to perform integration efficiently. As implemented in the previous works [12,13], we divide the q_0 integration into small ranges and integrate the quark propagator over $q_0^{(l)}\le q_0\le q_0^{(l+1)}$ ($q_0^{(1)}=-\Lambda_0, q_0^{(N)}=\Lambda_0$) as

$$M^{11}(P)\simeq-\frac{iC_{\rm F}}{2\pi^2}\int_\delta^\Lambda dq\frac{q}{p}\sum_{l=1}^{N-1}\langle\alpha_{\rm s}J_{11}(q)\rangle_l[MI_{11}(q_0^{(l+1)},q_0^{(l)})] \tag{2.17}$$

with

$$\begin{aligned}[MI_{11}(q_0^{(l+1)},q_0^{(l)})]&=[(MI_{\rm F})(q_0^{(l+1)},q_0^{(l)})]_{\rm R}\\&\quad+i[(MI_{\rm F})(q_0^{(l+1)},q_0^{(l)})]_{\rm I}N_{\rm F}(T,\langle q_0\rangle_l),\end{aligned} \tag{2.18}$$

where the remaining contributions of the integrand are averaged over the range $q_0^{(l)}\le q_0\le q_0^{(l+1)}$. Here, $\langle X\rangle_l$ denotes the average of a function $X(q_0)$ at $q_0=q_0^{(l+1)}$ and $q_0=q_0^{(l)}$ as $\langle X\rangle_l=[X(q_0^{(l+1)})+X(q_0^{(l)})]/2$. The explicit expressions are summarized in Appendix A, in which we implement the running coupling constant for $\alpha_{\rm s}$.

3. Numerical results

In this section, some numerical results are presented. We solve the SDE presented in Eq. (2.17) by a recursion method starting from a constant mass at $T=0$.[2]

First, we evaluate an effective quark mass for the resonance peak of the effective quark propagator at $T=0$. The denominator of the effective quark propagator is written as

$$D_{\rm F}(P)=(P^2-(M^2)_{\rm R})^2+((M^2)_{\rm I})^2 \tag{3.1}$$

in our approximation, which gives the resonance peak at $P^2=(M^2)_{\rm R}$.

For each iteration, we calculate the quark mass function normalized as

$$M^{(n+1)}(P^2)=m(\zeta^2)+M^{(n)}(P^2)-M^{(n)}(\zeta^2), \tag{3.2}$$

[2] The initial input parameters are $M_{\rm R}=\Lambda_{\rm QCD}$ and $M_{\rm I}=0$ at $T=0$ with $\Lambda_0=\Lambda=10\Lambda_{\rm QCD}$ and $\delta=0.1\Lambda_{\rm QCD}$ with $\varepsilon=10^{-6}$. In evaluation of the quark mass function at $T+\Delta T$, we implement the solution of M obtained at T as the initial input. Here, we define $M=M_{\rm R}+iM_{\rm I}$.

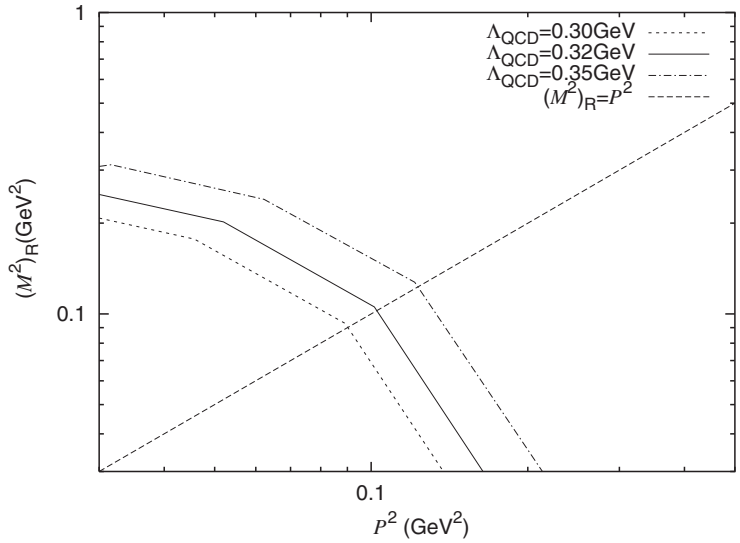

Fig. 1. The P^2 dependences of $(M^2)_{\rm R}$ for $P^2 > 0$ and $p_0 > \delta$ at $T = 0$ with the massless gluon. The dashed line denotes $(M^2)_{\rm R} = P^2$.

where n denotes the number of iterations. Here, the mass function is normalized by a current quark mass at large ζ^2, in which perturbative calculations are reliable. In the iteration, the mass function $M(p_0, p)$ in the integrand of Eq. (2.17) is replaced by the renormalized one obtained by the previous iteration. Here, $m(\zeta^2)$ is a renormalized mass at a renormalization scale ζ.[3]

Here, $M(P^2)$ is defined as

$$M(P^2) = M(p_0, \delta)\theta(|p_0| - \delta) \tag{3.3}$$

for $P^2 > 0$ with $p = \delta$, where $P^2 = p_0^2 - p^2$.

In Fig. 1, the P^2 dependences of the mass function $(M^2)_{\rm R}$ with $\Lambda_{\rm QCD} = 0.30\,{\rm GeV}$, $0.32\,{\rm GeV}$, and $0.35\,{\rm GeV}$ for a massless gluon ($m_{\rm T} = m_{\rm L} = 0$) are presented at $T = 0$. A dashed line denotes $(M^2)_{\rm R} = P^2$. Therefore, the crossed point corresponds to a position of the resonance peak of the effective quark propagator.

As shown in Fig. 1, the peak positions of the fermion propagator depend on the QCD parameter $\Lambda_{\rm QCD}$, which are roughly $\sqrt{(M^2)_{\rm R}} \simeq \Lambda_{\rm QCD}$ at $P^2 = (M^2)_{\rm R}$ in our model.

In order to search for the critical point at which the chiral symmetry is restored, we evaluate

$$\langle |M| \rangle = \int_{-\Lambda_0}^{\Lambda_0} dp_0 \int_{\delta}^{\Lambda} dp |M(p_0, p)|, \tag{3.4}$$

$$\langle M_{\rm R} \rangle = \int_{-\Lambda_0}^{\Lambda_0} dp_0 \int_{\delta}^{\Lambda} dp (M(p_0, p))_{\rm R} \tag{3.5}$$

and

$$\langle M_{\rm I} \rangle = \int_{-\Lambda_0}^{\Lambda_0} dp_0 \int_{\delta}^{\Lambda} dp (M(p_0, p))_{\rm I} \tag{3.6}$$

as order parameters.

[3] We take $m(\zeta^2) = 0$ at $\zeta = 10\Lambda_{\rm QCD}$.

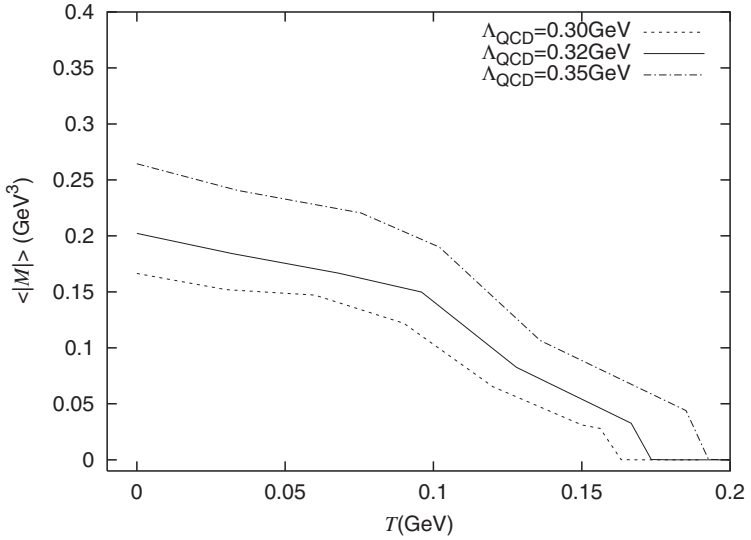

Fig. 2. The T dependences of the integrated quark mass functions $\langle|M|\rangle$ with $\Lambda_{\rm QCD} = 0.30\,\text{GeV}$, $0.32\,\text{GeV}$, and $0.35\,\text{GeV}$, respectively, with the massless gluon.

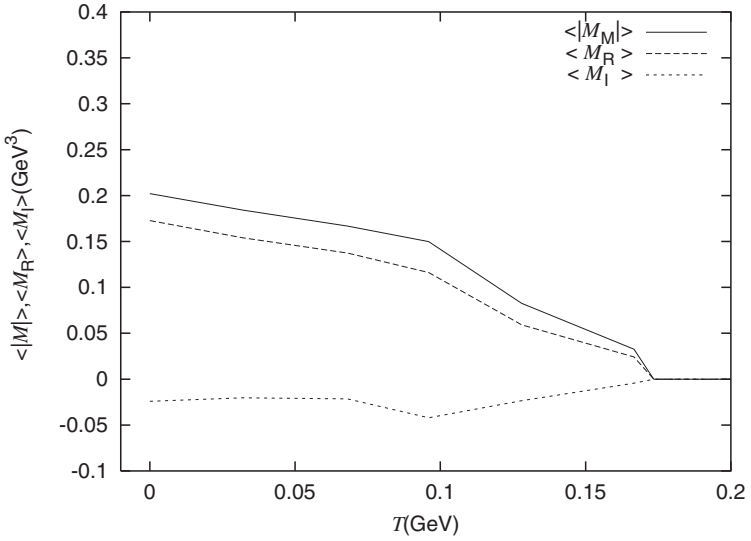

Fig. 3. The T dependences of the integrated quark mass functions $\langle|M|\rangle$, $\langle M_{\rm R}\rangle$, and $\langle M_{\rm I}\rangle$ at $\Lambda_{\rm QCD} = 0.32\,\text{GeV}$ with the massless gluon.

In Fig. 2, the T dependences of $\langle|M|\rangle$ for $\Lambda_{\rm QCD} = 0.30\,\text{GeV},\ 0.32\,\text{GeV}$, and $0.35\,\text{GeV}$ at $T = 0$ with the massless gluon are presented. The critical temperatures of the phase transition $T_{\rm C}$ depend on the QCD scale parameter $\Lambda_{\rm QCD}$. In our model, $0.3\,\text{GeV} \leq \Lambda_{\rm QCD} \leq 0.35\,\text{GeV}$ gives $0.16\,\text{GeV} \leq T_{\rm C} \leq 0.19\,\text{GeV}$, roughly $T_{\rm C} \sim \Lambda_{\rm QCD}/2$.

In Fig. 3, the T dependences of the integrated mass functions $\langle|M|\rangle$, $\langle M_{\rm R}\rangle$, and $\langle M_{\rm I}\rangle$ with the massless gluon are presented at $\Lambda_{\rm QCD} = 0.32\,\text{GeV}$, which gives $T_{\rm C} \simeq 0.175\,\text{GeV}$.

The gluon mass in the deep infrared region is nontrivial. Here, we consider two cases with the massive gluon in order to compare with the massless gluon case shown in Fig. 3. In Fig. 4, we present a case with $m_{\rm L} = \Lambda_{\rm QCD}$ and $m_{\rm T} = 0$ for $T > 0$, in which the longitudinal component of the gluon

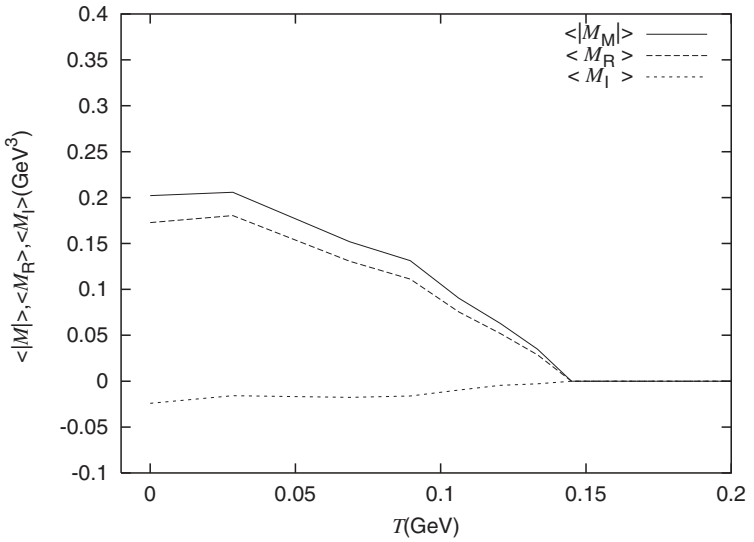

Fig. 4. The T dependences of the integrated quark mass functions $\langle|M|\rangle$, $\langle M_{\rm R}\rangle$, and $\langle M_{\rm I}\rangle$ at $\Lambda_{\rm QCD} = 0.32\,{\rm GeV}$ with $m_{\rm T} = 0$ and $m_{\rm L} = \Lambda_{\rm QCD}$.

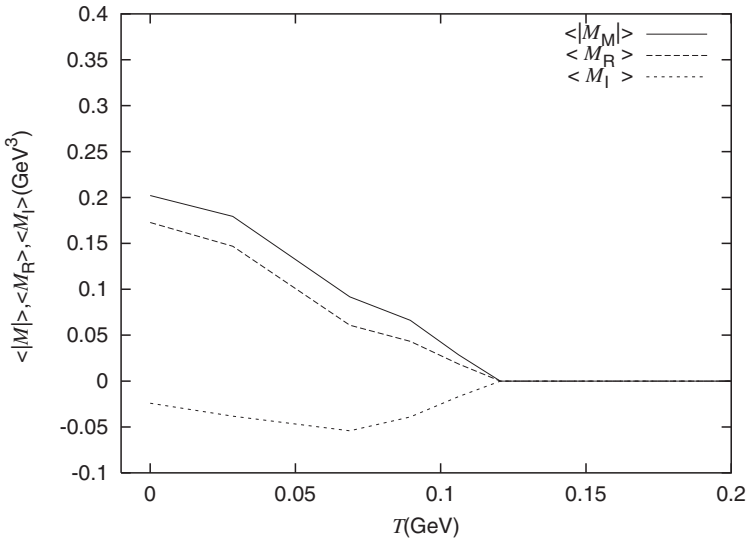

Fig. 5. The T dependences of the integrated quark mass functions $\langle|M|\rangle$, $\langle M_{\rm R}\rangle$, and $\langle M_{\rm I}\rangle$ at $\Lambda_{\rm QCD} = 0.32\,{\rm GeV}$ with gluon masses $m_{\rm T}$ and $m_{\rm L}$ extracted from lattice calculations.

propagator has an effective gluon mass $\Lambda_{\rm QCD}$. Another case is presented in Fig. 5, in which the gluon masses $m_{\rm T}$ and $m_{\rm L}$ for $T > 0$ are extracted from lattice calculations (see Appendix B).

As shown in these figures, though the critical temperatures depend on the gluon masses, the integrated quark mass functions are qualitatively similar behaviors in three cases, in which the imaginary parts of the mass functions $\langle M_{\rm I}\rangle$ have non-zero values for the broken chiral symmetric phase below the critical temperature $T_{\rm C}$, which means that the massive quark state may be unstable if the energy scale changes rapidly. Furthermore, the real and imaginary parts vanish at the same critical temperature. Therefore, when the temperature T approaches $T_{\rm C}$ in $T < T_{\rm C}$, the effective quark mass becomes smaller and the lifetime of the quasi-particle state may become longer due to the small imaginary part of the mass function.

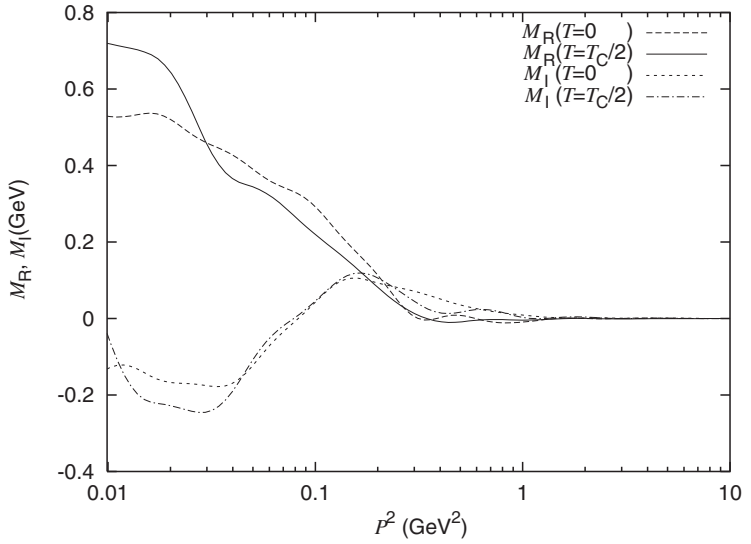

Fig. 6. The solid and dash-dotted curves denote the P^2 dependences of M_R and M_I for $P^2 > 0$ and $p_0 > 0$ with the massless gluon, respectively, at $T = T_C/2 = 8.75 \times 10^{-2}$ GeV. M_R and M_I at $T = 0$ with the massless gluon are represented by the dashed and dotted curves, respectively. Here, $\Lambda_{QCD} = 0.32$ GeV.

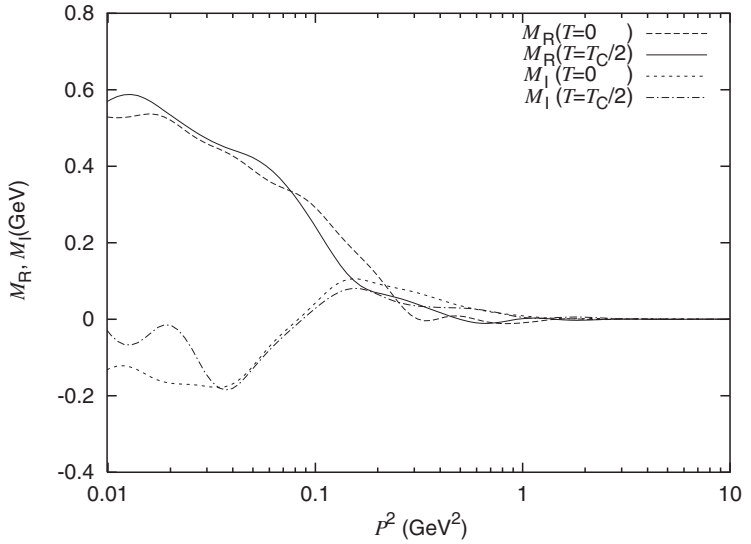

Fig. 7. The solid and dash-dotted curves denote the P^2 dependences of M_R and M_I for $P^2 > 0$ and $p_0 > 0$ with $m_L = \Lambda_{QCD}$ and $m_T = 0$, respectively, at $T = T_C/2 = 7.25 \times 10^{-2}$ GeV. M_R and M_I at $T = 0$ with the massless gluon are represented by the dashed and dotted curves, respectively. Here, $\Lambda_{QCD} = 0.32$ GeV.

In Figs. 6–8, P^2 dependences of M_R and M_I in Minkowski space at $T = 0$ and $T = T_C/2$ are presented for $P^2 > 0$ and $p_0 > 0$. As shown in these figures, M_I becomes positive in some regions of P^2, such as $P^2 > 0.1$ GeV^2. Similar behavior has been shown in Ref. [13].

4. Summary and comments

In this paper, we have studied quark mass functions solved by the Schwinger–Dyson equation (SDE) at finite temperature in the real-time formalism (RTF) without the instantaneous exchange approximation (IEA). The RTF enables us to evaluate nonequilibrium systems.

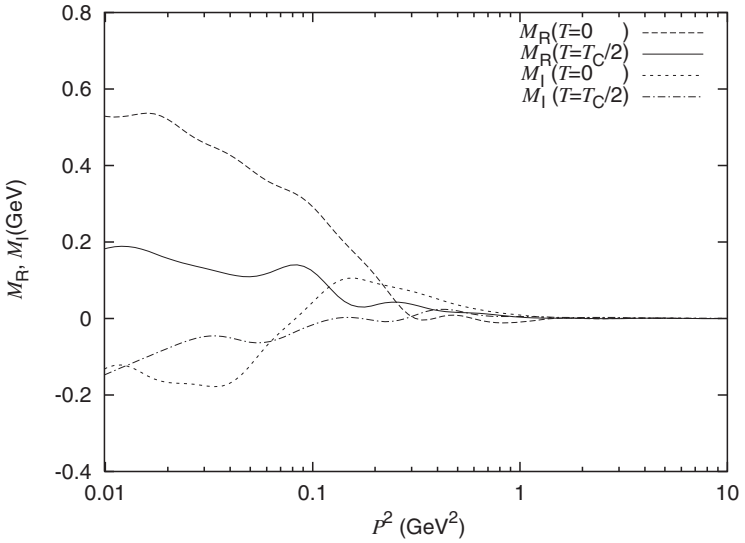

Fig. 8. The solid and dash-dotted curves denote the P^2 dependences of $M_{\rm R}$ and $M_{\rm I}$ for $P^2 > 0$ and $p_0 > 0$ with the gluon masses extracted from lattice calculations, respectively, at $T = T_{\rm C}/2 = 6.00 \times 10^{-2}$ GeV. $M_{\rm R}$ and $M_{\rm I}$ at $T = 0$ with the massless gluon are represented by the dashed and dotted curves, respectively. Here, $\Lambda_{\rm QCD} = 0.32$ GeV.

In our calculations, we improved the four-momentum integration of the SDE near the resonance peaks, which is one of the difficulties with numerical calculation in Minkowski space.

We defined integrated mass functions as order parameters and examined chiral symmetry restoration at finite temperature in the RTF. In our model, the critical temperature $T_{\rm C}$, in which the chiral symmetry is restored, depends on the gluon masses ($m_{\rm L}$ and $m_{\rm T}$) and the QCD scale parameter $\Lambda_{\rm QCD}$. Here, $m_{\rm L}$ and $m_{\rm T}$ denote the masses for a longitudinal component and a transverse component of the gluon propagator, respectively. Our model roughly gives the critical temperature for the chiral symmetry restoration $T_{\rm C} \sim \Lambda_{\rm QCD}/2$ at $T = 0$ with a massless gluon ($m_{\rm L} = m_{\rm T} = 0$), in which the the real part of the squared quark mass function $(M^2)_{\rm R}$ is given as $(M^2)_{\rm R} \simeq \Lambda^2_{\rm QCD}$. Here, $(M^2)_{\rm R}$ is determined by the resonance peak of the quark propagator. For example, $\Lambda_{\rm QCD} \simeq 0.32$ GeV gives $T_{\rm C} \simeq 0.175$ GeV with $\sqrt{(M^2)_{\rm R}} \simeq 0.32$ GeV for $P^2 = (M^2)_{\rm R}$ at $T = 0$.

The gluon mass at finite temperature in the deep infrared region is nontrivial. In this paper, we investigated two cases in order to compare the massless gluon case. We have presented the results for $T \geq 0$ with $m_{\rm L} = \Lambda_{\rm QCD}$ and $m_{\rm T} = 0$, and with the gluon masses extracted from lattice calculations. Though the critical temperature decreases for massive gluon cases compared to that with the massless gluon, our results give $0.12\,{\rm GeV} < T_{\rm C} < 0.18\,{\rm GeV}$, which may be qualitatively consistent with those obtained by lattice calculations [14–17].

We found that the imaginary part of the mass function $\langle M_{\rm I} \rangle$, which is the imaginary part of the mass function $M_{\rm I}$ integrated over the energy and momentum, is non-zero for the broken chiral symmetric phase below $T_{\rm C}$, which means that the massive quark state may be unstable if the energy scale of the system changes rapidly.

Furthermore, the real and imaginary parts of the integrated mass functions vanish at the same critical temperature. Therefore, when the temperature T approaches $T_{\rm C}$ in $T < T_{\rm C}$, the effective quark mass becomes smaller and the lifetime of the quasi-particle state may become longer due to the small imaginary part of the mass function.

In our calculations, the temperature dependences are not smooth curves. Therefore, we present crude dependences with few data points in order to search for the critical temperature of the chiral symmetry restoration. Within the present accuracy, we cannot determine the order of the phase transition.

We also evaluated the dependences of the squared four-momentum P^2 for the real and imaginary parts of the quark mass function. The imaginary part becomes positive in some regions of P^2, such as $P^2 > 0.1\,\mathrm{GeV}^2$. In conventional arguments in perturbation theories, the imaginary part of the energy for particles should be negative, since the imaginary part of the energy corresponds to the decay constant of the massive particle states. At $T = 0$, the positive value of M_I may break the positivity of the spectral function for the quark propagator [13]. It has been pointed out in Refs. [18–20] that the positivity violation of the spectral function for the quark and gluon contradicts the existence of asymptotic fields, which may imply confinement of the quark and gluon.

At finite temperature, we also found that M_I has a positive value for $P^2 > 0.1\,\mathrm{GeV}^2$, which depends on the effective gluon mass.

We may also expect a similar situation for the cases at $T = 0$, in which the positivity violation of the spectral function at finite temperature may imply a signature of quark confinement [21], which depends on the effective gluon mass. Therefore, the gluon mass may indirectly relate to the properties of the quark confinement.

Though the model presented in this paper is too simple to evaluate the quark mass function quantitatively, our study suggests that the SDE in the RTF without the IEA seems to be useful to investigate the chiral phase transition in QCD at finite temperature, in which we may directly evaluate the instability of the massive quark state and the signature of quark confinement.

Evaluations of the quark mass function at finite density are difficult in the imaginary-time formalism due to the sign problem, particularly in lattice simulations. In future work, we shall try to extend our method to evaluate the quark mass function at finite density in the RTF.

Acknowledgements

This work was partially supported by the MEXT-Supported Program for the Strategic Research Foundation at Private Universities, 2014-2017 (S1411024).

Funding

Open Access funding: SCOAP[3].

Appendix A. Formulas for numerical calculations

The quark mass function is given by

$$M^{11}(p_0,p) = -\frac{iC_\mathrm{F}}{2\pi^2}\int_{-\Lambda_0}^{\Lambda_0} dq_0 \int_\delta^\Lambda dq \frac{q}{p}[\alpha_\mathrm{s} M I_{11} J_{11}](p_0, p.q_0, q),$$

where the propagators I_{11} and J_{11} are defined in Eqs. (2.12) and (2.13), respectively.[4]

[4] In order to avoid the infrared contributions due to $M_\mathrm{I} = (M^{11})_\mathrm{I}/N_\mathrm{F}$ and N_B for small energy, we regularize the singularity of $\epsilon(x)\coth(x)$ as

$$\epsilon(x)\coth(x) \to \epsilon(x)\coth(x) - \left(\frac{1}{|x|} - \frac{1}{x_0}\right)\theta(x_0 - |x|)$$

with $x_0 = 0.1$, where x denotes $k_0/(2T)$ or $q_0/(2T)$.

As shown in Eq. (2.17), we approximate the integration over q_0 as

$$M^{11}(p_0,p) \simeq -\frac{iC_{\rm F}}{2\pi^2}\int_\delta^\Lambda dq\frac{q}{p}\sum_{l=1}^{N-1}\langle\alpha_{\rm s}J_{11}(q)\rangle_l[MI_{11}(q_0^{(l+1)},q_0^{(l)})]$$

with

$$[MI_{11}(q_0^{(l+1)},q_0^{(l)})] = [(MI_{\rm F})(q_0^{(l+1)},q_0^{(l)})]_{\rm R} + i[(MI_{\rm F})(q_0^{(l+1)},q_0^{(l)})]_{\rm I}N_{\rm F}(T,\langle q_0\rangle_l),$$

where $\langle X\rangle_l$ denotes an average of $X(q_0^{(l+1)})$ and $X(q_0^{(l)})$ as $\langle X\rangle_l = [X(q_0^{(l+1)}) + X(q_0^{(l)})]/2$.

Here, $[(MI_{\rm F})(q_0^{(l+1)},q_0^{(l)})]_{\rm R}$ and $[(MI_{\rm F})(q_0^{(l+1)},q_0^{(l)})]_{\rm I}$ are given as

$$[(MI_{\rm F})(q_0^{(l+1)},q_0^{(l)})]_{\rm R} \simeq \langle M_{\rm R}\rangle_l(I_{\rm F}(q_0^{(l+1)},q_0^{(l)}))_{\rm R} - \langle M_{\rm I}\rangle_l(I_{\rm F}(q_0^{(l+1)},q_0^{(l)}))_{\rm I}$$

and

$$[(MI_{\rm F})(q_0^{(l+1)},q_0^{(l)})]_{\rm I} \simeq \langle M_{\rm R}\rangle_l(I_{\rm F}(q_0^{(l+1)},q_0^{(l)}))_{\rm I} + \langle M_{\rm I}\rangle_l(I_{\rm F}(q_0^{(l+1)},q_0^{(l)}))_{\rm R}$$

respectively, with

$$I_{\rm F}(q_0^{(l+1)},q_0^{(l)}) = \int_{q_0^{(l)}}^{q_0^{(l+1)}} dq_0 I_{\rm F} = (I_{\rm F}(q_0^{(l+1)},q_0^{(l)}))_{\rm R} + i(I_{\rm F}(q_0^{(l+1)},q_0^{(l)}))_{\rm I}.$$

Here, the strong coupling constant $\alpha_{\rm s}$ is replaced by the running coupling constant $\alpha_{\rm s}(\bar{P}^2,\bar{Q}^2,T^2) = g_{\rm s}^2(\bar{P}^2,\bar{Q}^2,T^2)/(4\pi)$ [22], which is defined as

$$g_{\rm s}^2(\bar{P}^2,\bar{Q}^2,T^2) = \frac{1}{\beta_0}\times\left\{\begin{array}{ll}\frac{1}{t} & \text{if } t_{\rm F} < t \\ \frac{1}{t_{\rm F}} + \frac{(t_{\rm F}-t_{\rm C})^2-(t_{\rm C}-t)^2}{2t_{\rm F}^2(t_{\rm F}-t_{\rm C})} & \text{if } t_{\rm C} < t < t_{\rm F} \\ \frac{1}{t_{\rm F}} + \frac{(t_{\rm F}-t_{\rm C})}{2t_{\rm F}^2} & \text{if } t < t_{\rm C}\end{array}\right\}$$

with $\beta_0 = (33-2N_{\rm f})/(48\pi^2)$, $t = \log[(\bar{P}^2+\bar{Q}^2+T^2)/\Lambda_{\rm QCD}^2]$, $t_{\rm F} = 0.5$, and $t_{\rm C} = -2$ for $N_{\rm f} = 2$ flavors, where $\bar{P}^2 = p_0^2 + p^2$ and $\bar{Q}^2 = \langle q_0\rangle_l^2 + q^2$.[5]

For $I_{\rm F}$ and $J_{\rm F}$, we separate the real parts $(I_{\rm F})_{\rm R}, (J_{\rm F})_{\rm R}$ and the imaginary parts $(I_{\rm F})_{\rm I}, (J_{\rm F})_{\rm I}$, respectively.

For $J_{\rm F}$ in Eq. (2.14), we can integrate over k as

$$(J_{\rm F})_{\rm R} = (D_L)_{\rm R} + 2(D_T)_{\rm R}$$

with

$$(D_{\rm T/L})_{\rm R} = -\int_{\eta_-}^{\eta_+} dk\frac{k(k^2+m_{\rm T/L}^2-k_0^2)}{(k^2+m_{\rm T/L}^2-k_0^2)^2+\varepsilon^2} = -\frac{1}{4}\log\frac{(\eta_+^2+m_{\rm T/L}^2-k_0^2)^2+\varepsilon^2}{(\eta_-^2+m_{\rm T/L}^2-k_0^2)^2+\varepsilon^2}$$

and

$$(J_{\rm F})_{\rm I} = (D_{\rm L})_{\rm I} + 2(D_{\rm T})_{\rm I}$$

[5] We implement the QCD coupling constant $\alpha_{\rm s}$ with Euclidean momenta. The difference between the argument of $\alpha_{\rm s}$ with the momenta in Minkowski space and that in Euclidean space is part of the higher-order contributions to the one-loop approximation.

with

$$(D_{\mathrm{T/L}})_{\mathrm{I}} = -\int_{\eta_-}^{\eta_+} dk \frac{k\varepsilon}{(k^2 + m_{\mathrm{T/L}}^2 - k_0^2)^2 + \varepsilon^2}$$
$$= -\frac{1}{2}\left[\arctan\frac{\eta_+^2 + m_{\mathrm{T/L}}^2 - k_0^2}{\varepsilon} - \arctan\frac{\eta_-^2 + m_{\mathrm{T/L}}^2 - k_0^2}{\varepsilon}\right],$$

respectively, with $\eta_\pm = |p \pm q|$ and $k = |\mathbf{k}|$.

The real and imaginary parts of the quark propagator $I_{\mathrm{F}}(q_0^{(l+1)}, q_0^{(l)})$ are given by

$$(I_{\mathrm{F}}(q_0^{(l+1)}, q_0^{(l)}))_{\mathrm{R}} = \frac{\epsilon(\langle 2q_0 - \frac{\partial (E^2)_{\mathrm{R}}}{\partial q_0}\rangle_l)}{2\langle|2q_0 - \frac{\partial (E^2)_{\mathrm{R}}}{\partial q_0}|\rangle_l} \log\frac{[t_{\mathrm{R}}(q_0^{(l+1)}, q)]^2 + \langle (E^2)_{\mathrm{I}}\rangle_l^2}{[t_{\mathrm{R}}(q_0^{(l)}.q)]^2 + \langle (E^2)_{\mathrm{I}}\rangle_l^2}$$

and

$$(I_{\mathrm{F}}(q_0^{(l+1)}, q_0^{(l)}))_{\mathrm{R}} = \frac{\epsilon(\langle 2q_0 - \frac{\partial (E^2)_{\mathrm{R}}}{\partial q_0}\rangle_l)\epsilon(\langle (E^2)_{\mathrm{I}}\rangle_l)}{\langle|2q_0 - \frac{\partial (E^2)_{\mathrm{R}}}{\partial q_0}|\rangle_l}$$
$$\times\left[\arctan\frac{t_{\mathrm{R}}(q_0^{(l+1)}, q)}{|\langle (E^2)_{\mathrm{I}}\rangle_l|} - \arctan\frac{t_{\mathrm{R}}(q_0^{(l)}, q)}{|\langle (E^2)_{\mathrm{I}}\rangle_l|}\right],$$

respectively, with

$$t_{\mathrm{R}}(q_0, q) = q_0^2 - (E^2(q_0, q))_{\mathrm{R}},$$

where we define $\epsilon(z) = \theta(z) - \theta(-z)$ with the step function $\theta(z)$. Here, the real and imaginary parts of the squared energy denoted by $(E^2)_{\mathrm{R}}$ and $(E^2)_{\mathrm{I}}$, respectively, are given as

$$(E^2)_{\mathrm{R}} = q^2 + (M^2)_{\mathrm{R}}$$

and

$$(E^2)_{\mathrm{I}} = (M^2)_{\mathrm{I}} - \varepsilon,$$

with

$$(M^2)_{\mathrm{R}} = \mathrm{Re}(M^2) = (M_{\mathrm{R}})^2 - (M_{\mathrm{I}})^2$$

and

$$(M^2)_{\mathrm{I}} = \mathrm{Im}(M^2) = 2M_{\mathrm{R}}M_{\mathrm{I}}.$$

Appendix B. Effective gluon masses extracted from lattice calculation

We implement effective gluon masses for nonperturbative regions obtained by lattice calculation.

In Ref. [23], the longitudinal and transverse gluon propagators $D_{\mathrm{T/L}}(k^2)$ are defined by

$$D_{\mathrm{T/L}}(k^2) = \frac{c_{\mathrm{T/L}}(1 + d_{\mathrm{T/L}}k^2)}{(k^2 + r_{\mathrm{T/L}}^2)^2 + b_{\mathrm{T/L}}^2}$$

in the Landau gauge at the energy component of a Euclidean momentum $k_4 = 0$. The gluon propagator in Euclidean space may be written as

$$D_{\mathrm{T/L}}(k_4, k) = \frac{1}{k_4^2 + E_{\mathrm{T/L}}^2(k^2)}$$

with

$$E_{\mathrm{T/L}}^2(k^2) = \frac{1}{D_{\mathrm{T/L}}(k^2)}.$$

As an example of investigation for the gluon mass effects in SDE, we define the effective gluon masses as $m_{\mathrm{T/L}}^2 = E_{\mathrm{T/L}}^2(0)$ in this paper.

Here, the parameters $c_{\mathrm{T/L}}$, $d_{\mathrm{T/L}}$, $r_{\mathrm{T/L}}^2$, and $b_{\mathrm{T/L}}$ are obtained by lattice calculation in the Landau gauge, at the energy component of Euclidean space $k_4 = 0$.

These parameters below the critical temperature T_{C} do not strongly depend on the temperature. Therefore, we implement averaged values below T_{C} as

$$c_{\mathrm{L}} = 3.98, \;\; d_{\mathrm{L}} = 0.246, \;\; r_{\mathrm{L}}^2 = 0.321, \;\; b_{\mathrm{L}} = 0$$

and

$$c_{\mathrm{T}} = 5.42, \;\; d_{\mathrm{T}} = 0.156, \;\; r_{\mathrm{T}}^2 = 0.806, \;\; b_{\mathrm{T}} = 0,$$

respectively.

References

[1] F. J. Dyson, Phys. Rev. **75**, 1736 (1949).
[2] J. Schwinger, Proc. Nat. Acad. Sci. **37**, 452 (1951).
[3] V. Sauli, Towards the solution of Schwinger-Dyson equations in Minkowski space. *Ph.D. Thesis* (Faculty of Mathematics and Physics Charles University, 2005) [arXiv:hep-ph/0108160] [Search INSPIRE].
[4] P. Bicudo, Phys. Rev. D **69**, 074003 (2004) [arXiv:hep-ph/0312373] [Search INSPIRE].
[5] N. Dorey and N. E. Mavromatos, Phys. Lett. B **266**, 163 (1991).
[6] K. Fukazawa, T. Inagaki, S. Mukaigawa, and T. Muta, Prog. Theor. Phys. **105**, 979 (2001) [arXiv:hep-ph/9910305] [Search INSPIRE].
[7] T. Maskawa and H. Nakajima, Prog. Theor. Phys. **52**, 1326 (1974).
[8] T. Maskawa and H. Nakajima, Prog. Theor. Phys. **54**, 860 (1975).
[9] R. Fukuda and T. Kugo, Nucl. Phys. B **117**, 250 (1976).
[10] K.-I. Kondo and K. Yoshida, Int. J. Mod. Phys. A **10**, 199 (1995).
[11] H. Nakkagawa, H. Yokota, and K. Yoshida, arXiv:hep-ph/0703134 [Search INSPIRE].
[12] S. Sasagawa and H. Tanaka, Prog. Theor. Exp. Phys. **2017**, 013B04 (2017) [arXiv:1602.04291 [hep-ph]] [Search INSPIRE].
[13] H. Tanaka and S. Sasagawa, Prog. Theor. Exp. Phys. **2017**, 123B02 (2017) [arXiv:1705.09781 [hep-ph]] [Search INSPIRE].
[14] Y. Aoki, S. Borsányi, S. Dürr, Z. Fodor, S. D. Katz, S. Krieg, and K. Szabo, J. High Energy Phys. **0906**, 088 (2009) [arXiv:0903.4155 [hep-lat]] [Search INSPIRE].
[15] M. Cheng, N. H. Christ, M. Li, R. D. Mawhinney, D. Renfrew, P. Hegde, F. Karsch, M. Lin, and P. Vranas, Phys. Rev. D **81**, 054510 (2010) [arXiv:0911.3450 [hep-lat]] [Search INSPIRE].
[16] V. G. Bornyakov, R. Horsley, S. M. Morozov, Y. Nakamura, M. I. Polikarpov, P. E. L. Rakow, G. Schierholz, and T. Suzuki, [QCDSF-DIK Collaboration], Phys. Rev. D **82**, 014504 (2010) [arXiv:0910.2392 [hep-lat]] [Search INSPIRE].

[17] H.-T. Ding, P. Hegde, F. Karsch, A. Lahiri, S.-T. Li, S. Mukherjee, and P. Petreczky, Nucl. Phys. A **982**, 211 (2019) [arXiv:1807.05727 [hep-lat]] [Search INSPIRE].
[18] S. Strauss, C. S. Fischer, and C. Kellermann, Phys. Rev. Lett. **109**, 252001 (2012) [arXiv:1208.6239 [hep-ph]] [Search INSPIRE].
[19] D. Dudal, O. Oliveira, and P. J. Silva, Phys. Rev. D **89**, 014010 (2014) [arXiv:1310.4069 [hep-lat]] [Search INSPIRE].
[20] F. Siringo, Phys. Rev. D **94**, 114036 (2016) [arXiv:1605.07357 [hep-ph]] [Search INSPIRE].
[21] N. Su and K. Tywoniuk, Phys. Rev. Lett. **114**, 161601 (2015) [arXiv:1409.3203 [hep-ph]] [Search INSPIRE].
[22] Y. Taniguchi, and Y. Yoshida, Phys. Rev. **D55**, 2283 (1997).
[23] R. Aouane, V. G. Bornyakov, E.-M. Ilgenfritz, V. K. Mitrjushkin, M. Müller-Preussker, and A. Sternbeck, Phys. Rev. D **85**, 034501 (2012) [arXiv:1108.1735 [hep-lat]] [Search INSPIRE].